Oxidative Passivation of Metal Halide Perovskites

Julian S.W. Godding,[1] Alexandra J. Ramadan,[1] Yen-Hung Lin,[1] Kelly Schutt,[1] Henry J. Snaith,[1,*] and Bernard Wenger[1,2,*]

[1]Clarendon Laboratory, University of Oxford, Parks Road, Oxford OX1 3PU, U.K.
[2]Lead Contact
*Correspondence: bernard.wenger@physics.ox.ac.uk, henry.snaith@physics.ox.ac.uk

Graphical Abstract

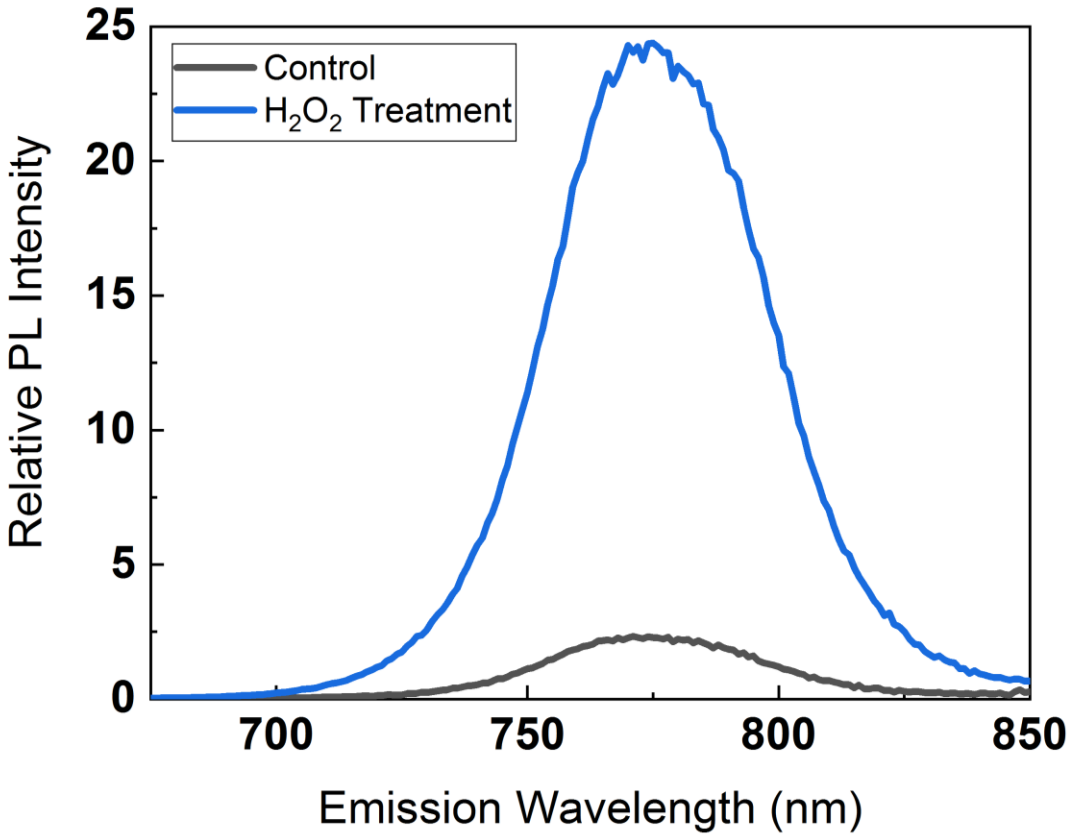

Blurb

The authors propose a comprehensive mechanism for the improvement to optoelectronic properties observed when metal halide perovskites are exposed to light and air in ambient conditions, a process known as photo-brightening. Hydrogen peroxide is shown to be the active reagent responsible and the authors demonstrate its use as a simple and fast post-treatment, resulting in substantial improvements to photoluminescence and photovoltaic device performance.

Highlights

- Discovery and characterisation of a simple, fast and scalable passivation technique using hydrogen peroxide.
- Photoluminescence quantum efficiency improvements of almost an order of magnitude
- 50 mV increases in open-circuit voltage for photovoltaic device scanned efficiencies.
- Inverted mixed-cation, mixed-halide perovskites with stabilised solar cell efficiencies of 19.2%

Context & Scale

Metal halide perovskites are being developed for an exciting new generation of optoelectronic devices including solar cells and LEDs. The need for clean and cheap energy generation has never been greater and perovskites have the potential to offer such a solution. However, there are several issues that must first be tackled. These include the unexplained improvement to optoelectronic properties when perovskites are exposed to light and air in ambient conditions, a process known as photo-brightening. Here, we show that oxidation occurring during exposure to ambient conditions reduces trap density with hydrogen peroxide as the active reagent. We demonstrate that hydrogen peroxide can be applied as a simple and scalable post-treatment to the perovskite, emulating the improvements observed during photo-brightening. This technique opens a new approach for perovskite chemical passivation, propelling their development for commercial application.

Summary

Metal halide perovskites have demonstrated extraordinary potential as materials for next-generation optoelectronics including photovoltaics and light-emitting diodes. Nevertheless, our understanding of this material is still far from being complete. One remaining puzzle is the phenomenon of perovskite ‘photo-brightening’; the increase in photoluminescence during exposure to light in ambient atmosphere. Here, we propose a comprehensive mechanism for the reactivity of the archetypal perovskite, $MAPbI_3$, in ambient conditions. We establish the formation of lead oxygen bonds by hydrogen peroxide as the key factor leading to perovskite photo-brightening. We demonstrate that hydrogen peroxide can be applied directly as an effective “post-treatment” to emulate the process and improve photoluminescence quantum efficiencies by nearly an order of magnitude. Finally, we show that the treatment can be incorporated into photovoltaic devices to give a 50 mV increase in open-circuit voltage,

delivering high 19.2 % steady-state power conversion efficiencies for inverted perovskite solar cells of the mixed halide, mixed cation perovskite $FA_{0.83}Cs_{0.17}Pb(I_{0.9}Br_{0.1})_3$.

Introduction

Within less than a decade, perovskites have emerged as pioneering next-generation photovoltaic materials due to their simple processing routes and power conversion efficiencies (PCE) that now surpass 23% in single junction cells, and 28 % in tandem cells with silicon.[1] However, whilst great strides have been made in photovoltaic performance, our understanding of the fundamental chemical reactivity of these organic-inorganic materials is still incomplete, with implications to their performance and long-term stability. "Light soaking" in air is often required to reach the highest efficiencies but the mechanism of this process is poorly understood and restricts the manufacture of high-performance photovoltaics under inert environments.

The effects of atmospheric conditions on the properties of the archetypal methylammonium (MA) lead iodide perovskite, $MAPbI_3$, have already been discussed extensively but remain topical issues. In particular, there is currently little consensus on whether the response of perovskites to oxygen and light in a humid environment is beneficial or detrimental to photovoltaic performance.

Reports have shown light soaking to reduce trap density, resulting in greater photoluminescence (PL),[2–5] but Gottesman *et al.* found the PL to actually decrease under these conditions.[6] The presence of oxygen has also been shown to enhance photoluminescence,[7,8] but Haque and co-workers propose the formation of a superoxide species from oxygen in air as initiating the degradation of $MAPbI_3$.[9] The presence of water has been shown to be crucial in controlling the crystallisation kinetics of the perovskite film, yet the hygroscopic nature of the organic cation is also believed to act as the pathway for water to initiate degradation.[10,11] Brenes *et al.* showed that increasing the humidity in air as $MAPbI_3$ is exposed to light, could lead to high photoluminescence quantum efficiencies (PLQE) and proposed that superoxide species played a positive role in this process.[12] Superoxide is a highly reactive species and very unlikely to be inert in a lattice environment of organic methylammonium species, interstitial iodide ions and under-coordinated lead, as demonstrated by Haque and co-workers.[9]

Despite some previous progress, a complete mechanistic understanding for the increase of PL efficiency under light soaking (hereafter called "photo-brightening") has not yet been proposed. Similarly to previous reports, we observe the process of photo-brightening to occur when $MAPbI_3$ is irradiated with above band gap illumination in ambient conditions (we show an example in **Figure S1**).[3,5,12,13] The photoluminescence increases by orders of magnitude over a period of several hours. Eventually, continuous illumination causes excessive degradation of the perovskite and the photoluminescence begins to fall; continuing to do so until complete breakdown of the material. Light treatment has been shown to be a determining factor for device performance and we believe that a full understanding of the process will be beneficial for applications of perovskite in optoelectronic devices.[5] Furthermore, knowledge of the mechanism may also lead to more practical and manufacturing-compatible routes to achieving the same result. Here we propose a complete mechanism for the photo-brightening of the metal halide perovskites, explaining the temporal changes to PL. We perform steady-state and time-resolved PL measurements, X-ray photoemission spectroscopy (XPS) and characterise photoluminescence quantum efficiencies to understand the nature of the passivation occurring and give further evidence to our proposed mechanism. We demonstrate that the active reagent of the process can be used in a post-treatment, mimicking the prolonged photo-brightening process within seconds. Finally, we show that the post-treatment gives substantial improvements to photovoltaic performance of perovskite solar cells.

Results and Discussion

Mechanism for Photo-brightening

In order for the absolute PL to rise, a passivation or elimination of non-radiative recombination centres must be occurring steadily during this process. In order to investigate what "passivating agent" is responsible for the photo-brightening, we consider the reactivity of $MAPbI_3$ in light, oxygen and water.

In 1967, Verwey examined the defect chemistry of lead halides and presented the following mechanism for their photochemical decomposition at room temperature, written in Kröger-Vink defect notation.[14] In this mechanism, the reaction is initiated by the generation of an electron-hole pair upon absorption of a photon. The photo-generated hole ($h^{\bullet}$) can combine with an iodide ion (I_I^X) to form an iodine atom ($I_I^{\bullet}$), as we show in reaction 1,

$$I_I^x + h^{\cdot} \rightarrow I_I^{\cdot} \quad (1)$$

It is plausible that this reaction occurs along with a rapid site exchange of the iodide from a regular to interstitial lattice site, as indicated by recent simulations of relaxation effects of defects in $MAPbI_3$.[15]

Two iodine atoms can combine to give an iodine molecule (I_2) - a volatile species which can then desorb from the surface to give two anion vacancies, as we illustrate in reaction 2.

$$2I_I^{\cdot} \rightarrow I_2(g) + 2V_I^{\cdot} \quad (2)$$

These vacancies may trap an electron ($e^{\cdot}$), forming a Farbe centre (F-centre), which can then reduce a lead cation on an adjacent site (Pb_{Pb}^x) to form Pb^+ ($Pb_{Pb}^{\prime}$), which we show in reactions 3 and 4 below,

$$V_I^{\cdot} + e^{\prime} \rightarrow (V_I^{\cdot} e^{\prime})^x \quad (3)$$

$$Pb_{Pb}^x + (V_I^{\cdot} e^{\prime})^x \rightarrow (V_I^{\cdot} Pb_{Pb}^{\prime})^x \quad (4)$$

A disproportionation reaction then occurs to generate atomic lead, $Pb_{Pb}^{\prime\prime}$, charge compensated by two anion vacancies ($V_I^{\cdot}$).

$$2Pb_{Pb}^{\prime} \rightarrow Pb_{Pb}^x + Pb_{Pb}^{\prime\prime}$$

If this same degradation mechanism can be applied to $MAPbI_3$ as suggested by Schoonman,[16] the generation of iodine should be detected from the perovskite film. Iodine gas release was successfully demonstrated by Kim *et al.*, strongly supporting the mechanism we have described above as the mechanism for the vacancy reactivity of the perovskite under light.[17] Detection of Pb^0 on the surface of the perovskite further supports this mechanism.[18]

The formation of superoxide species under illumination in the presence of oxygen was reported by Aristidou *et al.*[9] Due to the reactivity of superoxide as a strong proton scavenger and an initiator of radical reactions,[19] O_2^- will readily abstract the acidic proton on the MA cation if in

close proximity to the ammonium group to form a hydroperoxyl radical (HO_2•), as we show in equation 5 and 6.

$$O_2 + e^- \rightarrow O_2^- \quad (5)$$

$$CH_3NH_3^+ + O_2^- \leftrightarrow CH_3NH_{2(g)} + HO_2\bullet \quad (6)$$

We note that for this reaction to happen, oxygen does not need to be trapped in an iodide vacancy but can simply physisorb onto the surface.[20] This process generates methylamine that can easily escape in the gas phase, leaving lead iodide (PbI_2) and propagating degradation.

Following the formation of superoxide, hydrogen peroxide can be generated by either hydroperoxyl radical electron abstraction (eq. 7), the reaction with another hydroperoxyl (eq. 8) or the reaction of superoxide with water (eq. 9). Previous reports of improvement to PLQE moving from dry air to humid air and visible degradation of the perovskite by loss of MA suggest that all these processes, which we show in equations 7-9, are likely to be occurring while light soaking.[5,9]

$$HO_2\bullet + e^- \rightarrow HO_2^- \quad (7)$$

$$2HO_2\bullet \leftrightarrow O_2 + H_2O_2 \quad (8)$$

$$O_2^- + H_2O \rightarrow \tfrac{1}{2}\, O_2 + H_2O_2 \quad (9)$$

The introduction of oxygen to create superoxide species subsequently generates hydrogen peroxide, a strong oxidant in close proximity to a lead-rich surface. Infrared spectroscopy of products formed by the reaction of Pb with H_2O_2 has been performed in 2005 by Wang *et al.*, and revealed the enthalpically favourable formation of $Pb(OH)_2$.[21] We infer that this reactivity can also be applied to the atomic lead generated on the perovskite surface.

$$Pb + H_2O_2 \rightarrow Pb(OH)_2 \quad (10)$$

Ab initio simulations by Zhang *et al.* identified a pathway for the formation of PbO through the reaction of peroxide anions with lead octahedra in the perovskite lattice to form two covalent Pb-O bonds.[20] The distorted octahedra subsequently fragment to form PbO degradation products. Similarly, atomic lead on the perovskite surface can react with peroxide to generate localised PbO structures. This behaviour of reactivity is outlined in equation 11.

$$Pb + H_2O_2 \rightarrow PbO + H_2O \quad (11)$$

Recent XPS studies by Anaya *et al.* also detected the presence of PbO, after photoexcitation of $MAPbBr_3$ in an oxygen atmosphere. The lead oxide species were still present after hundreds of hours, revealing their irreversible generation. Anaya and co-workers suggested the formation of a peroxide ion via superoxide electron abstraction (prior to protonation in eq. 6) and we note that this may also be a competing pathway for its generation.[8] However, the study failed to identify the consequential passivating effects that result from the oxidation of atomic lead.

From these studies we infer the formation of lead-oxygen bond networks generated by the oxidation of metallic lead (Pb^0) at the surface (or grain boundaries) of a perovskite polycrystalline film. Reports have demonstrated Pb^0 as a donor-like surface state,[22] with Pb^0 acting as a quencher.[23] In the latter study, the quenching effect was inferred from the improvement in PL efficiency when the stoichiometry of $MAPbBr_3$ films was modified so as to prevent the formation of Pb^0. Oxidation of Pb^0 would provide effective passivation; explaining the improved PL efficiencies and device performance observed upon illumination in ambient conditions. Indeed, XPS studies (see Anaya et al.[8] and our own results shown below) are consistent with the presence of metallic lead being related to the temporal changes to PL upon exposure to oxygen and light.

However, we note that Pb^0 hasn't been identified as a non-radiative recombination centre from *ab initio* studies of defects in metal halide perovskites. Instead, oxidised interstitial iodide,[15,24,25] and reduced halogen vacancies,[26–28] have both been found to generate mid-gap trap states. Our mechanism is based on the defect chemistry proposed by Verwey et al. for PbI_2,[14] which assumes the presence of Schottky defects, leading to formation of halide vacancies. In $MAPbI_3$, reduced iodide vacancies (V_I^x and $V_I^{\cdot}$) induce the formation of Pb-Pb dimers which act as deep-level trap states due to their strong covalent character.[26–28] As noted above, the disproportionation of neighbouring oxidized lead species ($Pb_{Pb}^{\cdot}$) is required to generate Pb^0 and is accompanied by the formation of anion vacancies, which is consistent with the presence of the Pb-Pb dimers. Experimental evidence by Colella *et al.* for the generation of paramagnetic Pb^{3+} defects, potentially by the formation of Pb_2^{3+} dimers along with a reduced iodine vacancy, supports this.[29] Therefore, an alternative interpretation would be that the PL quenching species are actually the reduced halide vacancies (and associated dimers), where the presence of Pb^0 is a symptom, rather than the cause, of the quenching. The generation of PbO

would still lead to passivation, preventing the accumulation of anion vacancies and formation of Pb-Pb dimers.

It is also plausible that the oxidation of atomic lead can have indirect passivating outcomes through electrostatic repulsion. The formation of polar lead-oxygen bond networks on the surface (or grain boundaries) is coherent with previous suggestions of an electrostatically-induced interstitial iodide migration and defect annihilation.[2,8,30] Lead-oxygen bond formation could be the driving force responsible for the annihilation of iodide Frenkel pairs and migration of interstitial iodide away from the surface into lattice vacancies; reducing their contribution to non-radiative recombination pathways to give an improved photoluminescence.[30]

We note that hydroperoxyl radicals will be generated in the presence of any acid (eq. 6), providing a plausible explanation for the photo-brightening observed when acidic compounds are used as perovskite precursors or generated as bi-products during crystallisation, such as in the "acetate route".[5,31] The greater acidity of MA also explains why the process of photo-brightening is more frequently observed with MA as the A-site cation, as opposed to formamidinium or caesium, an observation which previous reports on photo-brightening have been unable to explain.

In summary, our proposed mechanism provides a comprehensive understanding of the reactivity of $MAPbI_3$ under ambient conditions and gives insights into the origins of instability in metal halide perovskites. The initial light-induced step generates atomic lead with loss of iodine, disturbing the stoichiometry of the perovskite and increasing the density of surface states responsible for charge recombination. Superoxide forms from oxygen physisorbed onto the surface under illumination and readily abstracts a proton from the methylammonium cation yielding peroxide. The peroxide reacts as a strong oxidising agent with the atomic lead, predominantly at the perovskite surface, to form Pb-O bond networks. Loss of the MA cation is harmful to optoelectronic performance whilst the generation of atomic lead appears to be crucial for effective oxidation. The oxidation process reduces the number of charge-trapping states and results in the observed photo-brightening. This whole process can occur on the timescale of several hours and is strictly dependent on the conditions of humidity in air and light intensity. At a critical point, highly dependent on the conditions of light intensity and humidity, degradation of the perovskite through loss of MA and formation of PbI_2 overtakes the passivating effect of oxidised PbO bond networks. The photoluminescence then starts to decrease and eventually the perovskite degrades entirely.

Oxidation with Hydrogen Peroxide

In order to test our proposed mechanism for photo brightening, we apply the active reagent, hydrogen peroxide, directly to the perovskite films as a post-treatment.

We explored two methods of H_2O_2 treatment; one solvent-based and the other via the gas phase, which we describe in detail in the Methods section. For the wet deposition method, we briefly dip a perovskite film into a low-concentration solution of H_2O_2 in isopropanol (IPA). Whereas, for the gas phase treatment, we use the Urea Hydrogen Peroxide (UHP) adduct to generate an atmosphere of H_2O_2 gas, to which we expose the perovskite in a chamber, as a close imitation of the reaction we propose in ambient conditions. We prepared thin films of $FA_{0.83}Cs_{0.17}Pb(I_{0.83}Br_{0.17})_3$ using an anti-solvent quenching route (see Methods), substituting MA for a less acidic A-site cation to diminish the possibility of in-situ generation of peroxide. This perovskite composition has also proved to be more stable in thin-film solar cells with reported device efficiencies that surpass 20%.[32,33]

First, we use PL spectroscopy to investigate the effects of the H_2O_2 post-treatments on the optoelectronic properties of the perovskite films. In **Figure 1a** and **1b**, we show steady-state and time-resolved PL measurements of thin films of $FA_{0.83}Cs_{0.17}Pb(I_{0.83}Br_{0.17})_3$ treated via the wet method.

To compare the different PL decays, we use $\tau_{e^{-1}}$, the time taken for the normalised intensity to reach e^{-1}, as an indicator of the decay lifetime. A longer lifetime indicates decreased non-radiative recombination, which is generally considered to indicate a higher quality material due to a reduced defect density. For films treated with 13 mM and 26 mM solutions of H_2O_2 in isopropanol, we obtain lifetimes of 140 ns and 281 ns respectively, which represents a significant increase compared to a mean control value of 40 ns (full decay shown in **Figure S2**). The measurements of radiative lifetime had an error of ± 5 ns. The time-integrated PL intensities show a more than 10x increase with the H_2O_2 treatment (**Figure 1b**). Both of these findings suggest a large reduction in non-radiative pathways, consistent with the passivation of defects at the surface. Interestingly, the initial fast component of the decay observed in the first 50 ns is almost completely eliminated with the high concentration treatment of H_2O_2. At the low excitation fluence used here (carrier density ~10^{15} cm^{-3}), this initial decay is likely to be related to fast trapping which is detrimental to the device performance.[12,34–37] To exclude that the improvement is due to the water contained in the peroxide solution, we performed a control

measurement with an equivalent concentration of water in IPA and observed no improvements to the PL, which we show in **Figure S3**.

Next, we measure the PL quantum efficiency as a function of irradiance for perovskite films treated via the gas deposition method for various treatment times between 0 and 180 s, and show the results in **Figure 1c**. We measure a maximum PLQE of 22.1% at 1.1 W/cm^2 irradiance for the films treated for 180 s, in comparison to 4.4% for the untreated control film. For all samples we observe a strong dependence of the PLQE on the excitation power, which is consistent with a trap-filling mechanism. However, H_2O_2 treated films evolve more quickly to high PLQE values and their high irradiance efficiency is significantly increased with increasing treatment time. This is once again consistent with increased radiative efficiency due to passivation of defect sites responsible for non-radiative recombination.

Finally, we compare the improvements to PLQE with H_2O_2 to other passivation treatments which currently act as the state-of-the-art, namely treatments with phenethylammonium iodide (PEAI) and butylammonium iodide (BAI).[38,39] In **Figure 1d**, we show the PLQE for films treated with the different passivation agents under 1 sun irradiance. We measure a PLQE of 6.4% at 1 sun irradiation for films treated with H_2O_2 for 60 s, in comparison to 1.4% for untreated films, 1.7% for BAI and 2.3% for PEAI. From this we conclude that the gas-phase H_2O_2 treatment is more effective than some of the current best performing passivation agents in reducing the concentration of defects leading to non-radiative recombination.

To be useful in solar cells, a passivation treatment needs to be able to sustain the thermal stresses that devices undergo in operating conditions. Therefore, we measure the PLQE for films treated with BAI, PEAI and H_2O_2 held at 85°C in an inert nitrogen atmosphere for over 100 hours and show the results in **Figure S4.** Much like BAI and PEAI, the PLQE for H_2O_2 treated films decreases rapidly, resulting in a value of about 1% after the first day. However, after this initial decrease it remains relatively stable and is still significantly higher than the control film which also degrades to give a PLQE of 0.3%. These results highlight that, although these passivation treatments provide initially large improvements to PLQE, the performance of treated films is negatively affected by heat. Thus, we infer that understanding and improving the thermal stability of passivated films will play an important role in the preparation of metal halide perovskite devices with both high radiative efficiency and long term operational stability.

Interestingly, we observed a significant visual change in appearance of the film, for films treated with higher concentrations of hydrogen peroxide, as we show in the photographs in **Figure S5.** From light absorption spectra, shown in **Figure S6**, we observe that the absorbance decreases slightly but the absorption onset remains constant after treatment, indicating that this effect is not due to a change in the band gap of the perovskite material. Further experiments confirm that the perovskite is degraded by prolonged exposure to H_2O_2 solutions (**Figure S7**), which we explain by the oxidation of formamidinium into volatile formamidine, leaving PbI_2. Thus, we attribute the colour change to an optical interference caused by the presence of a new thin layer forming on top of the perovskite surface with a different refractive index, which could be lead iodide or lead oxide. This interpretation is further supported by the observation of reaction products with broad featureless absorption spectra, upon prolonged treatments of PbI_2 films to H_2O_2 solution, which is consistent with the formation of PbO or PbO_2 (**Figure S8**). We show further X-ray diffractograms in **Figure S9**, which confirm that no structural change to the bulk perovskite crystal occurs, indicating that the treatment is primarily a surface effect when the films are exposed to low amounts of hydrogen peroxide, as in the gas phase method.

Additionally, we investigated the potential use of oxidative passivation on a pure inorganic perovskite, $CsPb(Br_{0.9}I_{0.1})_3$. According to our proposed mechanism, proton sources (such as MA or FA cations) are required for the in-situ generation of H_2O_2. Directly exposing the perovskites to hydrogen peroxide with our treatment should alleviate this dependence to proton sources. Indeed, when films of $CsPb(Br_{0.9}I_{0.1})_3$ were treated with H_2O_2 via the gas phase route for five minutes, steady-state PL measurements showed a five-times improvement compared to the control as shown in **Figure S10.**

In order to gain insight into the chemical nature of the perovskite surface before and after oxidative treatments, we carried out X-ray photoemission spectroscopy (XPS) measurements. We show high resolution scans of Pb 4*f* and O 1*s* in **Figure 2** and report high resolution scans for the regions corresponding to Br 3*d*, I 3*d* and Cs 3*d* and a full table of peak positions in **Figure S11** and **Table S1**, respectively. We observe no significant changes to the Br, I and Cs environments in both the pristine and treated films.

Pb 4*f* scans show peaks at 138.7 eV and ~137 eV, attributed to Pb^{2+} and Pb^0 respectively. These peaks are observed for all samples except those exposed to 10 minutes of treatment, in this case only one peak at 138.7 eV is observed. We observe that the loss of the peak corresponding to

Pb^0 (in the films which have undergone treatment for the longest time) is accompanied by a significant broadening of the Pb^{2+} peak, which we show in **Figure S12**. This suggests that the Pb^0 previously observed within the film is being oxidised to Pb^{2+} and the peak broadening observed is typical for metal oxide species.[18] O 1*s* scans for all samples show three oxygen peaks to be present within the surface of all thin films. These species are observed at ~533 eV, 531 eV and 530 eV, with slight variations in the exact peak position between samples. We attribute these to organic C=O (533 eV), peroxide O_2^{2-} / hydroxide OH^- (531 eV) and oxide O^{2-} (530 eV).[40] Peroxide and hydroxide O 1*s* peak positions are at very similar binding energies and we propose that both these species are contributing to the 531 eV peak due to their formation in equations 7-10 in the mechanism detailed above. Anaya *et al.* have previously suggested the presence of metal oxide in reports of perovskite films exposed to oxygen under light and there are convincing similarities between their reported O 1*s* scan and the data we present here.[8] All three species of oxygen are observed in our films but the relative ratios of the different species varies between pristine and treated films. It is important to note that we determine a signal corresponding to O^{2-} (*i.e.* PbO) in the O 1*s* scan of the pristine films, which arises due to the samples being prepared and stored in air. However, there is a significant increase in the signal for O^{2-} observed in the treated samples. This finding, combined with the loss of the peak attributed to Pb^0 in the Pb 4*f* scans, is consistent with the generation of lead oxide on the surface of the perovskite with hydrogen peroxide as the reagent responsible.

If the oxidation of the perovskite surface is responsible for the observed passivation, a similar effect should be achievable with alternative oxidation agents. We exposed our untreated $FA_{0.83}Cs_{0.17}Pb(I_{0.83}Br_{0.17})_3$ films to an oxygen plasma and, separately, $MAPbI_3$ films to an ozone atmosphere. With both treatments, we observe substantial increases of the PL lifetimes and intensities as we show in **Figures S14-16**. Interestingly the fast component in the PL decay, which we attributed earlier to fast non-radiative recombination, is almost entirely suppressed.

From these findings, we can conclude that hydrogen peroxide is performing an 'oxidative passivation' of atomic lead at the perovskite surface, forming covalent lead oxygen bonds. Using XPS, Zu *et al.* showed the presence and hole-trapping nature of atomic lead (Pb^0) on the surface of $MAPbI_3$, resulting in a quenched photoluminescence.[22] Hence, the passivating effect is the consumption of Pb^0 and conversion to Pb^{2+}. Encouragingly, this behaviour matches the reactivity for our proposed mechanism of photo-brightening in the equations above.

H_2O_2 treatment for photovoltaic devices

The beneficial effect of light exposure on photovoltaic devices during the fabrication process was first demonstrated by Brenes *et al.*[5] However, the process of light soaking in air requires conditions that are difficult to control and can't be performed on perovskites without the MA cation, limiting its scope to perovskite compositions with poor stability. By using H_2O_2 directly as the oxidising reagent, we propose a post-treatment that is scalable, cheap, non-toxic and highly effective. Therefore, we next demonstrate the practical use of this gas-phase treatment in photovoltaic devices in the both n-i-p and p-i-n configurations. We fabricated planar heterojunction solar cells on glass substrates with the following architectures:

- FTO/SnO_2/ $FA_{0.83}Cs_{0.17}Pb(I_{0.83}Br_{0.17})_3$ perovskite/spiro-OMeTAD/Ag (n-i-p)
- FTO/poly-TPD/$FA_{0.83}Cs_{0.17}Pb(I_{0.9}Br_{0.1})_3$ perovskite/PCBM/BCP/Ag (p-i-n)

We show the current-voltage (J-V) curves of the control devices and the devices treated with hydrogen peroxide via the gas phase method for p-i-n devices in **Figure 3** and n-i-p devices in **Figures S17**.

Champion p-i-n devices had the following scanned parameters; J_{sc} = 22.7 mA/cm^2, V_{oc} = 1.06 V, FF = 0.79, PCE = 19.0%. Treatment with Urea Hydrogen Peroxide resulted in 30 mV improvements to open-circuit voltage and increase in PCE by almost a whole percentage to 19.8%. UHP treated n-i-p devices typically caused a 50 mV increase in V_{oc} with champion devices improving from 1.11 V to 1.16 V and scanned PCE increasing from 18.7 % to 19.5%. There was little change to FF and J_{sc}. We summarise the average values of these parameters for several control devices and those treated with urea hydrogen peroxide in **Table 1**. Encouragingly, the steady-state power outputs of both devices also show improvement upon treatment with H_2O_2. Inverted cells show an improvement from 18.5% to 19.2% and n-i-p cells show a 0.7% improvement to 17.8%. The difference between JV determined efficiency and SPO is similar form both control and H_2O_2 treated films, similarly both cell types exhibit some degree of hysteresis, which we show in the JV curves we in **Figures S22-S23**.

Conclusions

In summary, we have derived a comprehensive explanation for the mechanism responsible for photo-brightening observed in metal halide perovskites, and in doing so devised a straightforward process for achieving the same results. Our mechanism presents the formation of lead oxide on the perovskite surface which acts to passivate the material, leading to the

observed improvements in photoluminescence. We postulate this to occur by the oxidation of hole-trapping atomic lead, Pb^0 to PbO. Our mechanism implies hydrogen peroxide, H_2O_2, to be the active oxidising reagent. We applied H_2O_2 as a fast, scalable and effective post-treatment to the perovskite surface, which controllably emulates the process of photo-brightening. The mechanism also highlights the instability of the methylammonium cation and the degradation route for perovskites that are exposed to light in ambient conditions. By directly applying H_2O_2 as a post-treatment on a metal halide perovskite with less acidic A-site cations (*e.g.* formamidinium and caesium), we are able to apply oxidative passivation to stable, high-efficiency perovskite compositions without the need for light soaking. This resulted in significant improvement to the open-circuit voltage and power-conversion efficiency in photovoltaic devices, demonstrating oxidative passivation as a valuable technique in the quest for high luminescence and photovoltaic performance. The technique is likely to open a new avenue for perovskite chemical passivation, as an alternative to molecular passivation, propelling their development for next-generation photovoltaics, LEDs and other optoelectronic devices.

Experimental Procedures

$FA_{0.83}Cs_{0.17}Pb(I_{0.83}Br_{0.17})_3$ perovskite thin films

$FA_{0.83}Cs_{0.17}Pb(I_{0.83}Br_{0.17})_3$ solutions were made with a 4:1 volume ratio DMF:DMSO and adding the following precursor salts to obtain a stoichiometric 1.45 M solution in the desired composition: formamidinium iodide (FAI) (GreatCell Solar), caesium iodide (CsI) (99.9 %, Alfa Aesar), lead iodide PbI_2 (99 %, TCI Chemicals), lead bromide ($PbBr_2$) (98 %, Alfa Aesar). Solutions were prepared on the same day as they were deposited. Films of perovskite were obtained by spin-coating in a two-step process; first at 1000 rpm for 10 s then at 6000 rpm for 35 s, acceleration of 2000 rpm/s. A solvent quench with anisole was performed 10s before the end of the spinning process followed by annealing at 100 °C for 30 minutes. Spectroscopy samples were fabricated on glass following a cleaning procedure consisting of a series of sonication steps; first in Hellmanex (5 % in deionised water), followed by neat deionised water then acetone and finally isopropanol. Substrates were then treated in a Model 42 Series UVO-Cleaner from Jelight Company for 10 min. Alternatively, substrates were exposed to O_2 plasma (Pico, Diener electronic) for 10 min.

All inorganic perovskite $CsPb(Br_{0.9}I_{0.1})_3$ thin films

$CsPb(I_{0.1}Br_{0.9})_3$ solutions were made in DMSO with a 0.5 M concentration using the following precursor salts: caesium iodide (CsI) (99.9 %, Alfa Aesar), lead iodide PbI_2 (99 %, Sigma-Aldrich), lead bromide ($PbBr_2$) (98 %, Alfa Aesar) and caesium bromide (99.9 %, Alfa Aesar). Solutions were prepared and stirred at room temperature 24 h prior to spin-coating. Films of perovskite were obtained by spin-coated on cleaned glass, in dry air, in a two-step process; first at 4000 rpm for 40 s, acceleration of 1000 rpm/s, then at 6000 rpm for 5 s, acceleration of 2000 rpm/s. A solvent quench with anisole was performed 8 s before the end of the spinning process. The resulting films were then annealed at 150 °C for 15 minutes.

$MAPbI_3$ perovskite thin films

$MAPbI_3$ in acetonitrile solution was prepared as described in 'A low viscocity, low boiling point, clean solvent system for the rapid crystallisation of highly specular perovskite films' by N. Noel et al.[41] Samples were dynamically spin-coated in a nitrogen glovebox at 2000 rpm for 45 s, then annealed at 100 °C for 60 minutes.

Hydrogen Peroxide Treatment

For the wet-deposition method, hydrogen peroxide solution (30 wt% in water, Sigma-Aldrich) was diluted in iso-propanol (IPA). Two beakers are prepared, one containing hydrogen peroxide diluted to various concentrations in 10 mL of IPA and a second beaker containing 80 mL of IPA. Substrates are dipped in the first beaker for 1 s and then washed in the second beaker for 2 s. They are then dried with a compressed air gun to remove any remaining solution.

For the gas-deposition method of hydrogen peroxide, we place 100 mg of Urea Hydrogen Peroxide adduct (> 97%, Sigma Aldrich) in a large, covered Petri dish to create a closed gas chamber which is heated to 60 °C with the perovskite substrate and left for various time intervals. No further annealing after treatment gave the maximum PLQE yield, see **Figure S22**, and was repeated for all measurments. The gas deposition method is summarised in **Figure S23**.

Oxygen Plasma Treatment

A low-pressure plasma system (Pico, Diener Electronic) was used for the oxygen plasma post-treatment on the perovskite. Substrates were pumped to vacuum for 5 minutes, then filled with

oxygen for another 5 minutes and finally plasma was generated and held for various times for post-treatment of the perovskite light-absorbing layer.

Ozone Treatment

An ozone generator (Ulsonix) supplied a gas flow of 30 ozone in oxygen which substrates were exposed to for varying time intervals.

BAI and PEAI Treatment

For the PEAI and BAI post-treatment, we dissolve 2 mg/ml PEAI (Dyesol) or 2 mg/ml BAI (Dyesol) in IPA which were kept stirring overnight. Prior to use, the solutions were filtered with 0.45 μm filter. On the as-deposited perovskite films, we spin the PEAI or BAI solution at 5000 rpm for 40 s. The films were then annealed at 100 °C for 2 minutes.

X-ray Photoemission Spectroscopy (XPS)

Thermo Scientific Kα X-Ray Photoelectron spectrometer was used to perform XPS measurements using a monochromated Al Kα X-Ray source at a take-off angle of 90°. The core level XPS spectra were recorded using a pass energy of 20 eV (resolution approximately 0.4 eV) from an analysis area of 300 μm x 300 μm. The spectrometer work function and binding energy scale were calibrated using the Fermi edge and 3*d* peak recorded from a polycrystalline silver (Ag) sample prior to the commencement of the experiments. Fitting procedures to extract peak positions and relative stoichiometry from the XPS data were carried out using Avantage XPS software suite.

Steady State and Time-Resolved Photoluminescence

Time-resolved PL measurements were acquired using a time-correlated single photon counting (TCSPC) setup (FluoTime 300, PicoQuant GmbH). Film samples were photoexcited using a 507 nm laser head (LDH-P-C-510, Pico Quant GmbH) pulsed at frequencies between 100 kHz - 40 MHz, with a pulse duration of 117 ps and fluence of 30 nJ/cm^{-2}. The samples were exposed to the pulsed light source until a stable photoemission was obtained. The PL was collected using a high resolution monochromator and hybrid photomultiplier detector assembly (PMA Hybrid 40, PicoQuant GmbH).

Relative intensity steady state photoluminescence spectra were measured with a Horiba Flurolog spectrofluorimeter. The exposed area and the position of the crystals were carefully controlled to achieve similar illumination and collection conditions. The excitation wavelength was 535 nm.

UV-Vis Absorption

Absorption spectra were recorded on a Varian Cary 300 UV-Vis spectrophotometer.

Photoluminescence Quantum Efficiency (PLQE)

PLQE values were determined following the method of De Mello *et al.*[42] using a 532 nm continuous wave laser excitation source (Roithner, RLTMLL-532 2 W) to illuminate a sample in an integrating sphere (Newport, 70682NS), and the laser scatter and PL were collected using a fibre-coupled spectrometer (Ocean Optics MayaPro). The beam intensity was modified using neutral density filters.

Scanning Electron Microscopy

A field emission scanning electron microscope (Hitachi S-4300) was used to acquire SEM images. The instrument uses an electron beam accelerated at 2.0 kV, enabling operation at a variety of currents.

Device Fabrication

Devices were fabricated using fluorine-doped tin oxide (FTO) coated glass (Pilkington) as the transparent electrode. FTO was etched with 2 M HCl and zinc powder to obtained the required electrode pattern. The substrate was then cleaned following the same cleaning procedure as spectroscopy slides.

For n-i-p devices, the electron-transport layer SnO_2 was prepared by dissolving $SnCl_4.5H_2O$ precursor in IPA (17.5 mg/ml) and stirring for 30 minutes before depositing via spin-coating onto FTO at 3000 rpm for 30 s. The film was then annealed at 100 °C for 20 minutes and then at 180 °C for 60 minutes. The substrates were then immersed into a chemical bath, which consisted of $SnCl_2 \cdot 2H_2O$ (Sigma-Aldrich) in deionised water (0.012 M), 20.7 mM urea (Sigma-Aldrich), 0.15 M HCl (Fisher scientific) and 2.87 μM 3-mercaptopropionic acid

(Sigma-Aldrich). The substrates were kept in an oven at 70 °C for 180 min, after which they were sonicated in deionised water for 2 minutes. They were then washed with ethanol and annealed at 180 °C for 60 min. The electron-blocking layer was deposited as a 85 mg/ml 2,2',7,7'-tetrakis-(N,N-di-p-methoxyphenylamine)9,9'-spirobifluorene (spiro-OMeTAD) (Lumtec) solution in chlorobenzene. 20 µl of a lithium bis(trifluoromethanesulfonyl)imide (Li-TFSI) (520 mg/ml solution in acetonitrile) and 33 µl of 4-tert-butylpyridine (TBP), were then added per 1 ml of spiro-OMeTAD solution. Spin-coating was carried out at 2000 rpm for 30 s. The samples were left to oxidise in a desiccator for at least 12 hours before testing in the solar simulator. 100 nm thick silver electrodes were then deposited under high vacuum (10^{-6} mbar) through a shadow mask.

For the p-i-n inverted devices, poly[N,N'-bis(4-butylphenyl)-N,N'-bisphenylbenzidine] (polyTPD, 1-Material) used as the hole transporting material was dissolved in toluene at a concentration of 1 mg/mL along with 20 wt% of 2,3,5,6-Tetrafluoro-7,7,8,8-tetracyanoquinodimethane (F4-TCNQ, Lumtec) whilst for the electron transporting materials, [6,6]-Phenyl-C61-butyric acid methyl ester (PC61BM, 99% Solenne BV) and bathocuproine (BCP, 98% Alfa Aesar)were dissolved in chlorobenzene and isopropanol at a concentration of 20 mg/mL and 0.5 mg/mL, respectively. The p-i-n perovskite solar cells were fabricated following the same processing parameters reported in our previous work,[43] except for that the perovskite absorber layer was deposited using a solvent-quenching method [i.e. dropping antisolvent anisole (400 µL) 10 s before the end of the spin-cast process]. In this work, only the perovskite absorber layer and the electron-transporting layers were processed in a nitrogen-filled glovebox (O_2, H_2O <1 ppm); the rest of the fabrication as well as the incomplete devices were processed and handled in ambient air. Finally, the inverted cells were completed by thermal evaporation of 70 nm of silver contacts under vacuum (10^{-6} mbar).

External Quantum Efficiency Measurements

External quantum efficiency (EQE) was measured via custom built Fourier transform photocurrent spectrometer based on a Bruker Vertex 80v Fourier Transform Interferometer. Devices were illuminated with an AM1.5 filtered solar simulator. Devices were calibrated to a Newport-calibrated reference silicon solar cell with known external quantum efficiency. The devices were masked with a metal aperture with a defined active area, 0.0919 cm^2.

Current-Voltage Characterisation

Solar cell performance was measured using a class AAB ABET sun 2000 solar simulator that was calibrated to give simulated AM 1.5 sunlight at an irradiance of 100 mW/cm^2 . The irradiance was calibrated using an NREL calibrated KG5-filtered silicon reference cell. Current-voltage curves were recorded using a sourcemeter (Keithley 2400). All solar cells were masked with a metal aperture that was used to define the active area of the devices, which in this case was 0.0925 cm^2.

X-ray Diffraction Measurement

Diffraction patterns were obtained with a Panalytical X-Pert Pro MPD using Cu K_α radiation. Samples were either thin films deposited on glass or powders mounted using a small amount of grease.

Acknowledgements

This project has received funding from the European Union's Horizon 2020 research and innovation programme under the Marie Sklodowska-Curie grant agreement No 706552. The research leading to these results has received funding from the European Union's Horizon 2020 research and innovation programme under grant agreement No. 763977 of the PerTPV project. Kelly Schutt thanks the Marshall Aid Commemoration Commission. A.J.R. and H.J.S. acknowledges the Engineering and Physical Sciences Research Council for funding grants EP/M005143 and EP/M015254/1.

Author Contributions

J.S.W.G. and B.W. performed and analysed photoluminescence measurements. A.J.R. and J.S.W.G. performed and analysed the XPS study. Y.H.L., K.S. and J.S.W.G. all assisted with photovoltaic device preparation and analysis. J.S.W.G. invented the deposition methods of hydrogen peroxide. B.W. and H.J.S. supervised the project, gave editorial input and revised the manuscript which was written by J.S.W.G.

Declarations of Interest

H.J.S. is a co-founder, Chief Scientific Officer and a Director of Oxford PV Ltd.

Oxford University has filed a patent related to the subject matter of this manuscript.

References

1. NREL. Best Research-Cell Efficiences Chart. (2018). Available at: www.nrel.gov/pv/assets/images/efficiency-chart-20180716.jpg. (Accessed: 20th August 2009)
2. deQuilettes, D. W. *et al.* Photo-induced halide redistribution in organic–inorganic perovskite films. *Nat. Commun.* **7**, 11683 (2016).
3. Tian, Y. *et al.* Mechanistic insights into perovskite photoluminescence enhancement: light curing with oxygen can boost yield thousandfold. *Phys. Chem. Chem. Phys.* **17**, 24978–24987 (2015).
4. Yamada, Y., Endo, M., Wakamiya, A. & Kanemitsu, Y. Spontaneous Defect Annihilation in CH 3 NH 3 PbI 3 Thin Films at Room Temperature Revealed by Time-Resolved Photoluminescence Spectroscopy. *J. Phys. Chem. Lett.* **6**, 482–486 (2015).
5. Brenes, R. *et al.* Metal Halide Perovskite Polycrystalline Films Exhibiting Properties of Single Crystals. *Joule* **1**, 155–167 (2017).
6. Gottesman, R. *et al.* Photoinduced Reversible Structural Transformations in Free-Standing CH 3 NH 3 PbI 3 Perovskite Films. *J. Phys. Chem. Lett.* **6**, 2332–2338 (2015).
7. Galisteo-López, J. F., Anaya, M., Calvo, M. E. & Míguez, H. Environmental Effects on the Photophysics of Organic–Inorganic Halide Perovskites. *J. Phys. Chem. Lett.* **6**, 2200–2205 (2015).
8. Anaya, M., Galisteo-López, J. F., Ernesto Calvo, M., Espinos, J. P. & Miguez Phys Chem Lett, H. J. Origin of Light Induced Photophysical Effects in Organic Metal Halide Perovskites in the Presence of Oxygen. (2018). doi:10.1021/acs.jpclett.8b01830
9. Aristidou, N. *et al.* The Role of Oxygen in the Degradation of Methylammonium Lead Trihalide Perovskite Photoactive Layers. *Angew. Chemie Int. Ed.* **54**, 8208–8212 (2015).
10. Pearson, A. J. *et al.* Oxygen Degradation in Mesoporous Al 2 O 3 /CH 3 NH 3 PbI 3- x Cl x Perovskite Solar Cells: Kinetics and Mechanisms. *Adv. Energy Mater.* **6**, 1600014 (2016).

11. Eperon, G. E. *et al.* The Importance of Moisture in Hybrid Lead Halide Perovskite Thin Film Fabrication. *ACS Nano* **9**, 9380–9393 (2015).

12. Brenes, R., Eames, C., Bulović, V., Islam, M. S. & Stranks, S. D. The Impact of Atmosphere on the Local Luminescence Properties of Metal Halide Perovskite Grains. *Adv. Mater.* **30**, 1706208 (2018).

13. Meggiolaro, D., Mosconi, E. & De Angelis, F. Mechanism of Reversible Trap Passivation by Molecular Oxygen in Lead-Halide Perovskites. *ACS Energy Lett.* **2**, 2794–2798 (2017).

14. Verwey, J. . F. Photochemical Processes in Lead Halides. (Utrecht University, 1967).

15. Li, W., Liu, J., Bai, F.-Q., Zhang, H.-X. & Prezhdo, O. V. Hole Trapping by Iodine Interstitial Defects Decreases Free Carrier Losses in Perovskite Solar Cells: A Time-Domain Ab Initio Study. *ACS Energy Lett.* **2**, 1270–1278 (2017).

16. Schoonman, J. Organic–inorganic lead halide perovskite solar cell materials: A possible stability problem. *Chem. Phys. Lett.* **619**, 193–195 (2015).

17. Kim, G. Y. *et al.* Large tunable photoeffect on ion conduction in halide perovskites and implications for photodecomposition. *Nat. Mater.* **17**, 445–449 (2018).

18. Ramadan, A. J., Rochford, L. A., Fearn, S. & Snaith, H. J. Processing Solvent-Dependent Electronic and Structural Properties of Cesium Lead Triiodide Thin Films. *J. Phys. Chem. Lett.* **8**, 4172–4176 (2017).

19. Sawyer, D. T. & Valentine, J. S. How super is superoxide? *Acc. Chem. Res.* **14**, 393–400 (1981).

20. Zhang, L. & Sit, P. H.-L. Ab initio study of the role of oxygen and excess electrons in the degradation of CH 3 NH 3 PbI 3. *J. Mater. Chem. A* **5**, 9042–9049 (2017).

21. Wang, X. & Andrews, L. Infrared Spectra of M(OH) 1,2,4 (M = Pb, Sn) in Solid Argon. *J. Phys. Chem. A* **109**, 9013–9020 (2005).

22. Zu, F. *et al.* Surface State Density Determines the Energy Level Alignment at Hybrid Perovskite/Electron Acceptors Interfaces. *ACS Appl. Mater. Interfaces* **9**, 41546–41552 (2017).

23. Cho, H. *et al.* Overcoming the electroluminescence efficiency limitations of perovskite light-emitting diodes. *Science* **350**, 1222–5 (2015).

24. Meggiolaro, D. *et al.* Iodine chemistry determines the defect tolerance of lead-halide perovskites. *Energy Environ. Sci.* **11**, 702–713 (2018).

25. Mosconi, E., Meggiolaro, D., Snaith, H. J., Stranks, S. D. & De Angelis, F. Light-induced annihilation of Frenkel defects in organo-lead halide perovskites. *Energy Environ. Sci.* **9**, 3180–3187 (2016).

26. Agiorgousis, M. L., Sun, Y.-Y., Zeng, H. & Zhang, S. Strong Covalency-Induced Recombination Centers in Perovskite Solar Cell Material CH 3 NH 3 PbI 3. *J. Am. Chem. Soc.* **136**, 14570–14575 (2014).

27. Zhang, L. & Sit, P. H.-L. Ab initio study of the dynamics of electron trapping and detrapping processes in the CH 3 NH 3 PbI 3 perovskite. *J. Mater. Chem. A* **7**, 2135–2147 (2019).

28. Li, W. *et al.* Control of Charge Recombination in Perovskites by Oxidation State of Halide Vacancy. *J. Am. Chem. Soc.* **140**, 15753–15763 (2018).

29. Colella, S. *et al.* Light-Induced Formation of Pb 3+ Paramagnetic Species in Lead Halide Perovskites. *ACS Energy Lett.* **3**, 1840–1847 (2018).

30. Motti, S. G. *et al.* Controlling competing photochemical reactions stabilizes perovskite solar cells. *Nat. Photonics* 1 (2019). doi:10.1038/s41566-019-0435-1

31. Zhang, W. *et al.* Enhanced optoelectronic quality of perovskite thin films with hypophosphorous acid for planar heterojunction solar cells. *Nat. Commun.* **6**, 10030 (2015).

32. Petrus, M. L. *et al.* New Generation Hole Transporting Materials for Perovskite Solar Cells: Amide-Based Small-Molecules with Nonconjugated Backbones. *Adv. Energy Mater.* **8**, 1–11 (2018).

33. Ramirez, D. *et al.* Meso-superstructured perovskite solar cells: Revealing the role of the mesoporous layer. *J. Phys. Chem. C* **122**, 21239–21247 (2018).

34. Chen, Q. *et al.* Controllable Self-Induced Passivation of Hybrid Lead Iodide Perovskites toward High Performance Solar Cells. *Nano Lett.* **14**, 4158–4163 (2014).

35. Son, D.-Y. *et al.* Self-formed grain boundary healing layer for highly efficient CH3 NH3 PbI3 perovskite solar cells. *Nat. Energy* **1**, 16081 (2016).

36. deQuilettes, D. W. *et al.* Impact of microstructure on local carrier lifetime in perovskite solar cells. *Science* **348**, 683–6 (2015).

37. deQuilettes, D. W. *et al.* Tracking Photoexcited Carriers in Hybrid Perovskite Semiconductors: Trap-Dominated Spatial Heterogeneity and Diffusion. *ACS Nano* **11**, 11488–11496 (2017).

38. Lin, Y. *et al.* Enhanced Thermal Stability in Perovskite Solar Cells by Assembling 2D/3D Stacking Structures. *J. Phys. Chem. Lett.* **9**, 654–658 (2018).

39. Yoo, H.-S. & Park, N.-G. Post-treatment of perovskite film with phenylalkylammonium iodide for hysteresis-less perovskite solar cells. *Sol. Energy Mater. Sol. Cells* **179**, 57–65 (2018).

40. Briggs, D. Handbook of X-ray Photoelectron Spectroscopy C. D. Wanger, W. M. Riggs, L. E. Davis, J. F. Moulder and G. E.Muilenberg Perkin-Elmer Corp., Physical Electronics Division, Eden Prairie, Minnesota, USA, 1979. 190 pp. $195. *Surf. Interface Anal.* **3**, v–v (1981).

41. Noel, N. K. *et al.* A low viscosity, low boiling point, clean solvent system for the rapid crystallisation of highly specular perovskite films. *Energy Environ. Sci.* **10**, 145–152 (2017).

42. de Mello, J. C., Wittmann, H. F. & Friend, R. H. An improved experimental determination of external photoluminescence quantum efficiency. *Adv. Mater.* **9**, 230–232 (1997).

43. Jacob, T.-W. W. *et al.* Efficient perovskite solar cells by metal ion doping. *Energy Environ. Sci.* **9**, 2892–2901 (2016).

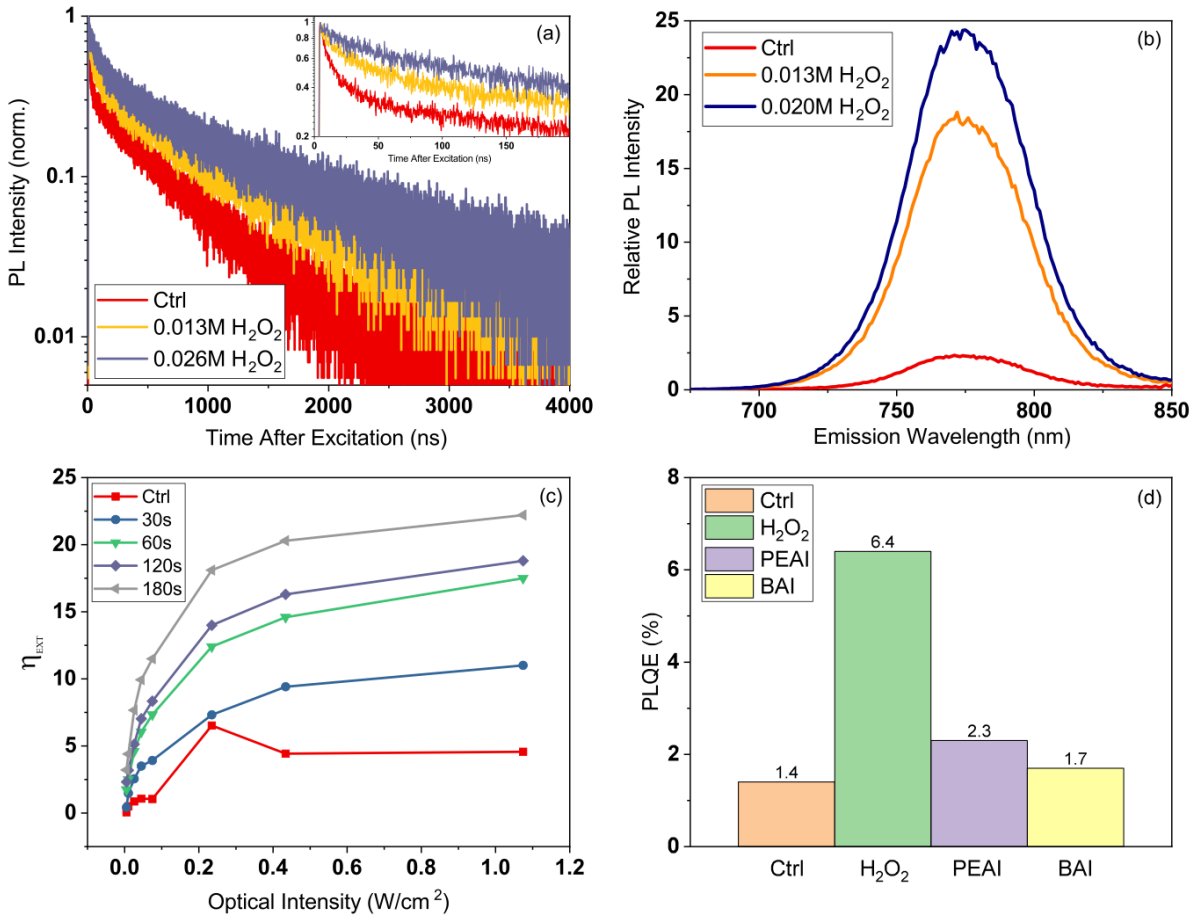

Figure 1 *Time-resolved* ***(a)*** *and steady state* ***(b)*** *photoluminescence measurements of control and treated films of* $FA_{0.83}Cs_{0.17}Pb(I_{0.83}Br_{0.17})_3$ *treated in low concentrations of* H_2O_2 *in IPA via the wet deposition method.* ***(c)*** *Intensity dependence of external PLQE values for films of* $FA_{0.83}Cs_{0.17}Pb(I_{0.83}Br_{0.17})_3$ *treated with* H_2O_2 *via the gas deposition method using Urea Hydrogen Peroxide.* ***(d)*** *PLQE of films of* $FA_{0.83}Cs_{0.17}Pb(I_{0.83}Br_{0.17})$ *after three different treatments;* H_2O_2 *(gas deposition for 60s), PEAI and BAI (see methods) under 1 sun intensity.*

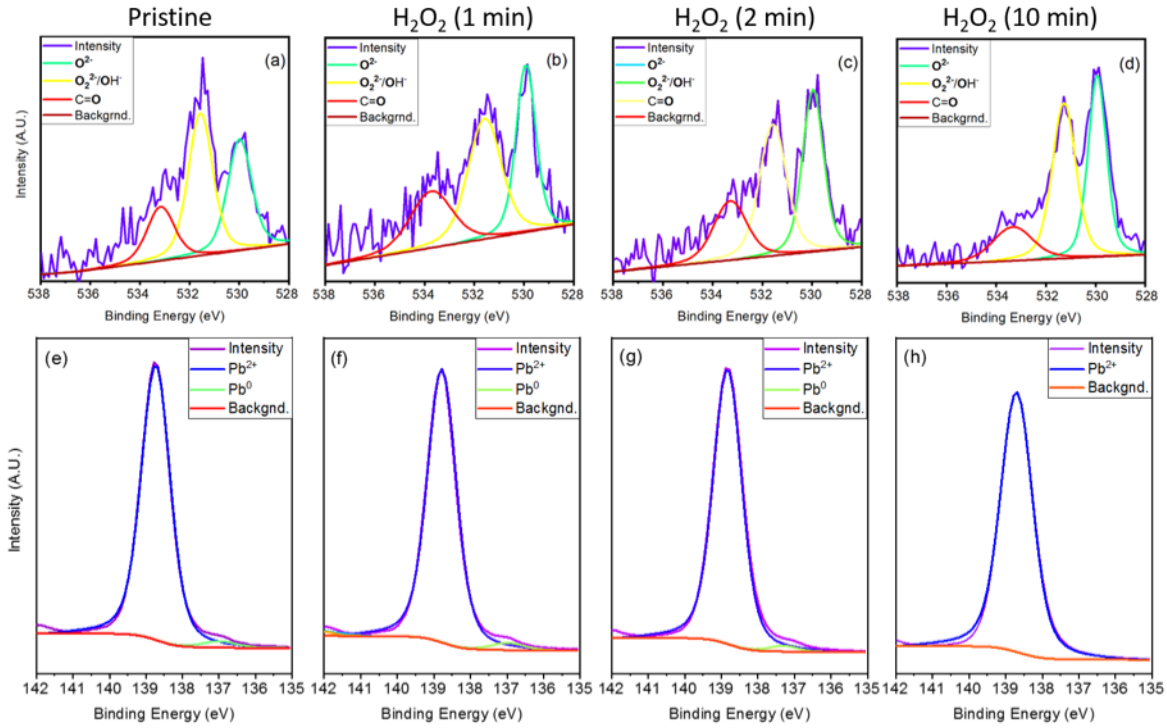

Figure 2 *- X-ray photoemission spectroscopy measurements of control and treated films of* $FA_{0.83}Cs_{0.17}Pb(I_{0.83}Br_{0.17})_3$*. The top and bottom rows of graphs show high resolution O 1s and Pb* $4f_{7/2}$ *scans of* ***(a, e)*** *pristine films,* ***(b, f)*** *films after 1 minute of treatment,* ***(c, g)*** *films after 2 minutes of treatment and* ***(d, h)*** *films after 10 minutes of treatment. The measured data are shown as the purple enveloping curves, and the fitted individual components of* Pb^{2+}*,* Pb^0 *and background, are shown as the blue, turquoise and red curves respectively.*

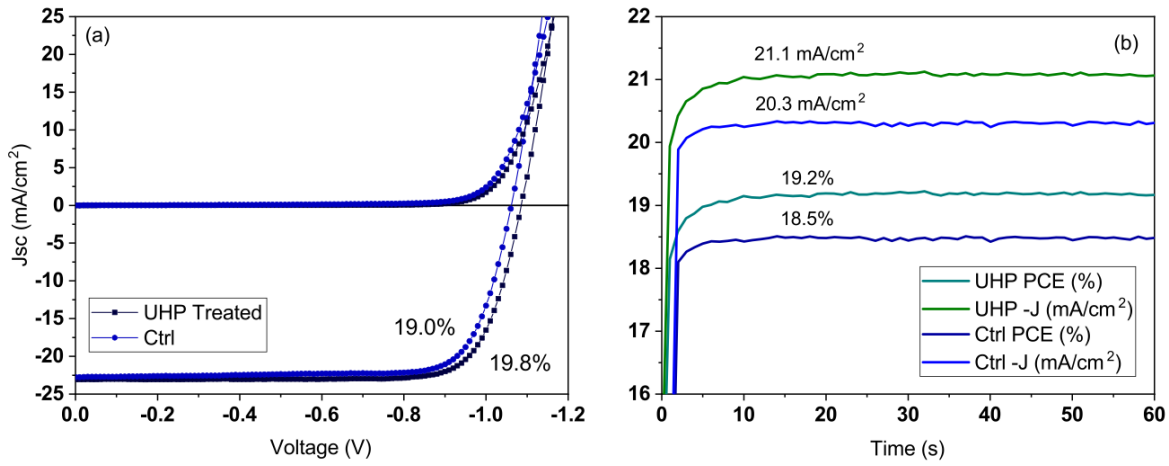

Figure 3 *- Current density–voltage (J–V) characteristics of photovoltaic devices treated by* H_2O_2 *via the gas-phase deposition method with urea hydrogen peroxide for 40 s, compared to a control device, measured under AM1.5 100 mW/cm*^{2} *simulated sunlight.* ***(a)*** *Current -voltage characteristics of the champion p-i-n devices in the light and dark.* ***(b)*** *Steady-state photocurrents and efficiencies of the p-i-n devices. Steady-state measurements were taken by holding the devices at their JV determined maximum power point for one minute.*

Table 1 *– Performance parameters of 24 pixels (on 4 separate substrates) each for n-i-p and inverted p-i-n configuration devices treated with Hydrogen Peroxide via the gas deposition method compared to control. SPO given is for the champion pixel.*

	J_{sc} (mA/cm^2)	PCE (%)	V_{oc} (V)	FF	SPO (%)
n-i-p Control	21.9 ± 0.4	17.6 ± 0.4	1.09 ± 0.01	0.73 ± 0.03	17.1
n-i-p Treated	21.7 ± 0.6	18.6 ± 1.0	1.13 ± 0.01	0.75 ± 0.03	17.8
p-i-n Control	21.9 ± 0.7	16.5 ± 1.2	-1.04 ± 0.01	0.70 ± 0.5	18.5
p-i-n Treated	22.1 ± 0.6	17.4 ± 1.1	-1.06 ± 0.01	0.71 ± 0.5	19.2